Lattice vacancies responsible for the linear dependence of the low-temperature heat capacity of insulating materials

Jacob M. Schliesser and Brian F. Woodfield*

Department of Chemistry and Biochemistry, Brigham Young University, Provo, Utah 84602, USA

(Received 14 June 2014; revised manuscript received 7 January 2015; published 29 January 2015)

The linear dependence on temperature (γT) of the heat capacity at low temperatures ($T < 15$ K) is traditionally attributed to conduction electrons in metals; however, many insulators also exhibit a linear dependence that has been attributed to a variety of other physical properties. The property most commonly used to justify the presence of this linear dependence is lattice vacancies, but a correlation between these two properties has never been shown, to our knowledge. We have devised a theory that justifies a linear heat capacity as a result of lattice vacancies, and we provide measured values and data from the literature to support our arguments. We postulate that many small Schottky anomalies are produced by a puckering of the lattice around these vacancies, and variations in the lattice caused by position or proximity to some form of structure result in a distribution of Schottky anomalies with different energies. We present a mathematical model to describe these anomalies and their distribution based on literature data that ultimately results in a linear heat capacity. From these calculations, a quantitative relationship between the linear term and the concentration of lattice vacancies is identified, and we verify these calculations using values of γ and vacancy concentrations for several materials. We have compiled many values of γ and vacancy concentrations from the literature which show several significant trends that provide further evidence for our theory.

DOI: 10.1103/PhysRevB.91.024109 PACS number(s): 65.40.Ba, 65.60.+a, 61.72.jd

I. INTRODUCTION

A. Linear heat capacity at low temperatures

Traditionally, the linear dependence of the low-temperature ($T < 15$ K) heat capacity has been associated with conduction electrons in metals [1,2], but a linear term γT has been found in many nonmetallic materials as well [3–5]. The linear dependence of these materials has been an area of great interest and has resulted in a number of theories having broad and often inconsistent origins.

In metals, the linear dependence arises from electrons that populate energy levels above the Fermi level at any finite temperature [1,2]. High-temperature ceramic superconductors have been found to show a linear dependence in the heat capacity. This could easily be misinterpreted as arising from conduction electrons similar to those in metals, but because the conductivity arises from Cooper pairs [6], which behave as bosons rather than fermions, new theories were needed to explain the linear dependence.

Many theories suggested the linear dependence was intrinsic to superconductivity [4,7–10], while others have attributed the linear term to a tunneling system related to oxygen [11], impurity phases such as $BaCuO_2$ in $YBa_2Cu_3O_7$ (YBCO) [12], or twin boundaries and oxygen vacancies [13–15]. The arguments of those against an intrinsic linear term are that linear terms are inconsistent from sample to sample and depend strongly on sample quality [4,10]; furthermore, some superconductors that become insulators at certain stiochiometries retain a similar linear term in the heat capacity even as insulators [16,17].

Several studies have attempted to identify the origins of the linear terms in insulating materials resulting in theories as diverse as the samples. Table I lists the linear terms of several insulating materials as determined from a combination of adiabatic [18–25], semiadiabatic pulse [19–23,26–30], isothermal [21,26], and relaxation calorimetry methods [5,18,21,27,31–43], and Fig. 1 graphically shows a sampling of these linear terms relative to each other. The linear term in $BaCuO_2$ has been attributed to magnetic degrees of freedom [23] but has also been disregarded simply because it is an insulator [44]. Nanocrystalline magnetite (Fe_3O_4) and hematite (Fe_2O_3) have linear terms that have been attributed to superparamagnetism [19,31]. The linear terms in several vanadium bronzes have been attributed to singlet bipolarons [24]. In several insulating layered oxides, the linear terms are attributed to a localized density of states associated with lattice vacancies [5]. Many investigations of insulators with linear terms adopt some form of this latter explanation since lattice vacancies are inherent to all materials to some degree; however, the only derivation of a linear heat capacity from lattice vacancies treats the vacancies the same as a free-electron gas where vacancies "move practically freely through a crystal", which is wholly unsupported in the paper by Andreev and Lifshits [45].

In glasses, the linear dependence on the low-temperature heat capacity has been attributed to particles trapped in defect sites that create a particle-in-a-box system [46,47], but a more common theory is based on a system of tunneling states [3,48,49]. This theory assumes that there are two equilibrium orientations that atoms or groups of atoms can have. The two energy minima associated with each of these orientations are separated by an energy barrier that must be overcome by phonon-assisted tunneling in order for the atoms to shift from one orientation to the other. The separation in energy between the two minima is different for every group of atoms because of local strains and the local configuration of the atoms around the group. Each of these two-level systems (TLS) for which the tunneling barrier is not too large results in a Schottky anomaly

*brian_woodfield@byu.edu

TABLE I. Linear terms from fits to the low-temperature ($T < 15$ K) heat capacity data. Materials in the nanophase are represented by (n). Units of γ are millijoules per mole per Kelvin.

Sample	γ	Sample	γ	Sample	γ
CuO [18]	0.022	γ-Al_2O_3 (n) [41]	1.354 2	$Sr_2TiSi_2O_8$ [40]	0.080 3
CuO (n)[a]	0.489	γ-Al_2O_3 (n) [41]	1.390 5	$BaCuO_2$ [23]	10.6
ZnO (n) [38]	0.103	γ-Al_2O_3 (n) [41]	1.22	$BaCuO_2$ [23]	12.4
Co/ZnO [38]	31.64	γ-Al_2O_3 (n) [41]	1.391 2	$BaCuO_{2.14}$ [23]	5.7
Co/ZnO (n) [38]	21.635	SnO_2 [37]	0.172	$Li_{1.2}Ti_{1.8}O_4$ [16]	3.6
$GeCo_2O_4$ [21]	0.33	SnO_2 (n) [37]	0.401	$Na_{0.25}V_2O_5$ [24]	11.3
CoO [20]	0.4	HfO_2 [39]	0.079 3	$Na_{0.28}V_2O_5$ [24]	9.42
CoO [38]	0.185 6	γ-FeOOH [27]	0.092 7	$Na_{0.33}V_2O_5$ [24]	9.85
CoO (n) [20]	6.0	γ-FeOOH [27]	0.352 6	$Na_{0.40}V_2O_5$ [24]	5.73
Co_3O_4[a]	2.138	β-FeOOH [27]	0.144 9	$K_{0.20}V_2O_5$ [24]	15.2
Co_3O_4 (n)[a]	8.46	2-line FeOOH [32]	0.155 1	$Cu_{0.40}V_2O_5$ [24]	60.1
Co_3O_4 (n)[a]	14.111	α-FeOOH [26]	0.23	$Cu_{0.55}V_2O_5$ [24]	32.5
TiO_2 rut [22]	0.099 3	α-Fe_2O_3 [33]	0.036 2	$Cu_{0.60}V_2O_5$ [24]	26.4
TiO_2 ana [22]	0.109 9	α-Fe_2O_3 [33]	0.022 4	$Ag_{0.33}V_2O_5$ [24]	8.05
TiO_2 rut (n) [29]	0.508	α-Fe_2O_3 (n) [31]	1.023 5	$La_{1.98}Ba_{0.02}CuO_4$ [17]	0.5
TiO_2 rut (n) [29]	0.564	Fe_3O_4 (n) [19]	3.461 9	$La_{0.7}Ca_{0.3}MnO_3$ [25]	5.2
TiO_2 rut (n) [29]	0.499 4	$FePO_4$ [36]	13.211	$La_{0.7}Ba_{0.3}MnO_3$ [25]	6.1
TiO_2 ana (n) [30]	0.594 1	Fe_3PO_7 [35]	16.32	$La_{0.7}Sr_{0.3}MnO_3$ [25]	6.0
TiO_2 ana (n) [30]	0.656 4	$Fe_3(P_2O_7)_2$ [36]	26.613	$Y_{0.7}Sr_{0.3}MnO_3$ [25]	8.1
TiO_2 ana (n) [30]	0.687 7	$Fe_4(P_2O_7)_3$ [35]	73.69	α-D-xylose [43]	0.490 2
$Ti_{0.78}Al_{0.22}O_2$ (n) [42]	0.811 8	$Fe_2P_2O_7$ [34]	83.61	Muskovite [5]	25.5
$Ti_{0.5}Al_{0.5}O_2$ (n) [42]	1.101	SiO_2 [28]	0.066		

[a]Linear terms and data to be published elsewhere.

in the low-temperature heat capacity [1]

$$C_{\mathrm{Sch}} = n_{\mathrm{Sch}}(\theta)k\left(\frac{\theta}{T}\right)^2 \frac{e^{\theta/T}}{(1+e^{\theta/T})^2}\,, \tag{1}$$

where θ is the energy separation of the two states with units of Kelvin ($\theta = \Delta E/k$), $n_{\mathrm{Sch}}(\theta)$ is the moles of anomalies per mole of material for a given separation θ, and k is the Boltzmann constant. Because the number and energies of these tunneling systems are random, the distribution $n_{\mathrm{Sch}}(\theta)$ can be assumed to be a constant value $n(0)$, which makes the sum of all Schottky anomalies approximated by the integral [3]

$$C_{\mathrm{lin}}(T) = \int_0^\infty n_{\mathrm{Sch}}(\theta)k\left(\frac{\theta}{T}\right)^2 \frac{e^{\theta/T}}{(1+e^{\theta/T})^2}d\theta \approx \frac{\pi^2}{6}k^2 n(0)T\,, \tag{2}$$

where $n(0)$ is the number of contributing TLSs per mole of sample per unit energy. As seen in Eq. (2), the heat capacity contribution from these TLSs is linear with temperature.

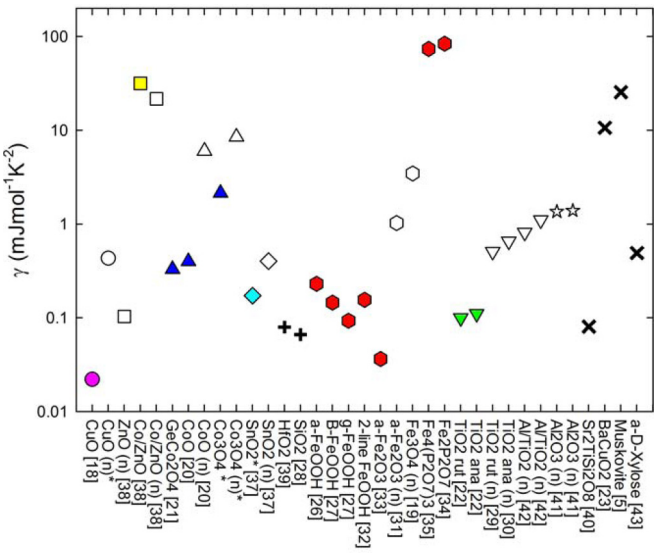

FIG. 1. (Color online) Selected linear terms γ from fits to the low-temperature ($T < 15$ K) heat capacity data of insulating materials. Hollow symbols represent the nanophase of the material; solid represents bulk.

The paper by Anderson *et al.* [3] outlining this theory provides no support for the use of a TLS believed to produce a Schottky anomaly or justification for a random distribution of energies produced by the TLSs. Several others have recognized this and have attempted to provide evidence for these properties, while others have modified the model to make the TLS and distribution more meaningful [11,24,50,51]. A major flaw in this theory is this lack of understanding of the source and distribution of the TLSs.

To understand the distribution, one must first understand the heat capacity that is produced by it. The linear heat capacity in metals exists up to high temperatures [O(1000 K)] but is generally undetectable due to the much larger contribution from phonons at temperatures any higher than about 15 K; however, the linear term in insulating materials does not extend up to high temperatures, and the extent to which the linear term is nonzero/nonnegligible has been investigated by several groups. Anderson *et al.* [3] claimed that the linear term of glasses must exist up to about 10 K before vanishing.

Investigations of $BaCuO_2$ have shown that this contribution to the heat capacity remains linear until about 30 K, where it begins to decrease until becoming negligible around 40 to 50 K [23,44]. Others investigating the heat capacity of $Fe_2P_2O_7$ claim that the linear term begins to decrease between 15–20 K [34]. The study by McWhan *et al.* [51] of several doped Al_2O_3 compounds shows linearity until about 25 K, above which the slope (γ) quickly decreases to zero. Data of TiO_2 from Sandin and Keesom [52] show an excess heat capacity that increases approximately linearly until about 15 K, then quickly drops to zero by about 20 K. Therefore, we will consider the shape of this excess heat capacity to be linear up to about 15 K, at which point, it decreases until becoming negligible around 50 K.

The broad range of insulating materials that have a linear heat capacity and the relatively similar cutoff temperature of these linear terms suggest that there exists a common underlying factor in all of these materials that produces the linear dependence in the low-temperature heat capacity.

B. Lattice vacancies

Lattice vacancies appear in all materials to some degree. At thermal equilibrium, the concentration of vacancies can be estimated using the Boltzmann factor (for $n_{\text{vac}} \ll N$) [2]

$$\frac{n_{\text{vac}}}{N} \cong \exp\left(-\frac{E_v}{kT}\right), \tag{3}$$

where n_{vac}/N is the ratio of the number of lattice vacancies n_{vac} to the number of atoms N, E_v is the energy required to remove an atom from the lattice site inside the crystal and place it on the surface, k is Boltzmann's constant, and T is the temperature of the crystal or the temperature at which the crystal was calcined if it was suddenly cooled (thereby freezing in vacancies). For a typical E_v (about 1 eV) and calcination temperature (about 1000 K), Eq. (3) yields a concentration of lattice vacancies on the order of 10^{-5} moles of vacancies per mole of atoms.

Lattice vacancies are generally determined using redox titrations or thermogravimetric analysis (TGA) [53–59], but for nanomaterials and materials with very few vacancies, less conventional methods are required such as extended x-ray absorption fine structure (EXAFS) [60,61], x-ray absorption near edge structure (XANES) [61], other x-ray techniques [53,61], Raman spectroscopy [60,61], high-resolution transmission electron microscopy (TEM) [61], electron energy loss spectroscopy (EELS) [62], x-ray energy dispersive spectroscopy (XEDS) [63], scanning transmission electron microscopy (STEM) [64], neutron diffraction [53,59], and a plethora of esoteric techniques [65–73]. Each of these methods is limited by experimental error, resolution, or applicability that constrain what samples can be tested and the amount of useful information that can be obtained (hence the large number of specialized techniques). The detection limit for most of these techniques is around parts per thousand or $n_{\text{vac}}/N \approx 10^{-3}$, making these techniques only suitable for highly nonstoichiometric samples. Table II lists lattice vacancy concentrations of a wide range of materials as measured from these techniques [57–62,64–74].

When a lattice vacancy is present in a crystal, the atomic structure around the vacancy takes on one of two possible conformations: dimer or puckered [74–77]. Each of these conformations has an energy minimum separated by an energy barrier. These two energy levels would result in a Schottky anomaly in the low-temperature heat capacity [Eqn. (1)] with an energy separation θ equal to the difference between the two levels. Surface configurations, which are somewhat similar to vacancies due to their similar coordinations and strain, have been shown to have similar TLSs that produce Schottky anomalies [78–81].

The energies of the dimer and puckered configurations of amorphous SiO_2 have been investigated by Boero *et al.* [75] using first principles calculations approximating the two levels to be separated by an energy difference of about 0.25 eV. Skuja [82] reviewed several articles on spectroscopic methods

TABLE II. Measured lattice vacancy concentrations for several materials. Values of n_{vac} have been converted into moles of vacancy per mole of formula unit.

Sample	n_{vac}	Sample	n_{vac}
C doped TiO_2 [65]	1.12×10^{-3}	CeO_2 (5 nm) [60]	6.01×10^{-3}
C doped TiO_2 [65]	0.017 6	CeO_2 (10 nm) [60]	2.4×10^{-3}
TiO_2 as prepared [65]	9.41×10^{-4}	CeO_2 (10 nm) [66]	2.0×10^{-3}
TiO_2 oxidized [65]	2.01×10^{-5}	CeO_2 (15 nm) [68]	2.4×10^{-4}
Fe doped TiO_2 [61]	6.27×10^{-3}	CeO_2 (20 nm) [60]	1.2×10^{-4}
Cr doped $SrTiO_3$ [67]	6.6×10^{-4}	CeO_2 (30 nm) [60]	2.4×10^{-5}
$LaSrCoO_x$ [64]	0.25	CeO_2 (65 nm) [60]	1.2×10^{-5}
$Sr_2MgMoO_{(6-\delta)}$ [58]	0.05	Fe_3O_4 [73]	4.9×10^{-3}
$Ba_{0.5}Sr_{0.5}Co_{0.8}Fe_{0.2}O_{(3-\delta)}$ [59]	0.661	Fe_3O_4 (10 nm) [70]	0.036
$Ba_{0.5}Sr_{0.5}Co_{0.8}Fe_{0.2}O_{(3-\delta)}$ [59]	0.807	Fe_3O_4 (n)[a]	0.1250
$Ce_{0.9}Gd_{0.1}O_{1.95}$ [69]	0.13	CuO [71]	6.2×10^{-4}
$La_{0.67}Ca_{0.33}MnO_{(3-y)}$ [62]	0.065	CuO [57]	9.8×10^{-4}
MgO $3.5Al_2O_3$ [72]	0.072	CuO (n)[a]	0.0109
Co_3O_4[a]	9.5×10^{-3}	Cu_2O [57]	7.3×10^{-4}
Co_3O_4 (n)[a]	0.1230	SiO_2 [74]	$\sim 3 \times 10^{-4}$
CoO (n)[a]	0.1639	Al_2O_3 (n)[a]	4.7×10^{-3}

[a]This study.

used to investigate energies associated with vacancies and showed that a spectrum of energy levels up to 0.1 eV arises from vacancies in a typical solid. Rigid unit modes of SiO_4 tetrahedra have TLSs similar to lattice vacancies and have a range of possible energies up to around 500 GHz or about 2 meV [83]. Di Valentin *et al.* [79] investigated tunneling related to rotations of surface atoms and found tunneling barriers between about 10 and 20 meV. Gryaznov *et al.* [84] discovered lattice vacancy energy levels with energies around 20 meV different from the lattice. Smith [80] investigated librational frequencies covering the range of 30 peV to 33.5 meV. Strong librational frequencies around oxygen vacancies in perovskites have been found to have energies of about 90–120 cm^{-1} (11–15 meV), and a broad spectrum of peaks below 90 cm^{-1} have been attributed to thermally induced disorder, which essentially consists of lattice vacancies as Eq. (3) shows [85]. From all these investigations, we conclude that energies associated with lattice vacancies have a broad distribution of possible states, likely caused by differences in the lattice surrounding each vacancy, and have an average maximum of about 20 meV.

From the information presented above, it can be seen that a single lattice vacancy results in a TLS that is capable of producing a Schottky anomaly in the low-temperature heat capacity. Multiple vacancies have a random distribution of energy differences that would yield a distribution of Schottky anomalies. The cutoff of the energies from the TLSs would also produce a cutoff (albeit gradual) in the sum of the Schottky anomalies produced from the vacancies. We will show how the energies associated with TLSs are responsible for the linear term and its cutoff temperature and matches what has been observed experimentally.

II. THEORY AND CORRELATIONS

A. Distributions

We first consider the distribution of energies associated with the TLSs from vacancies that determine $n_{\mathrm{Sch}}(\theta)$ in Eq. (2). The distribution $n_{\mathrm{Sch}}(\theta)$ used for Eq. (2) assumes that n_{Sch} is a single value for all values of θ up to infinity, but we will examine several other possible and more meaningful distributions that correspond to the experimental data outlined above and that could produce a linear (or pseudolinear) heat capacity with an appropriate ending temperature. All of the following distributions have been tailored so that $n_{\mathrm{Sch}}(\theta)$ is negligible by about 150 K (or 13 meV). These distributions use θ with units of Kelvin rather than milli-electron volts to be applicable to the Schottky heat capacity as given in Eq. (1). We note here that 1 meV = 11.6 K.

Figure 2 shows several hypothetical distributions of $n_{\mathrm{Sch}}(\theta)$. A simple Gaussian distribution with θ_{max} centered at 30 K and a standard deviation of 40 K is shown in Fig. 2(a). In

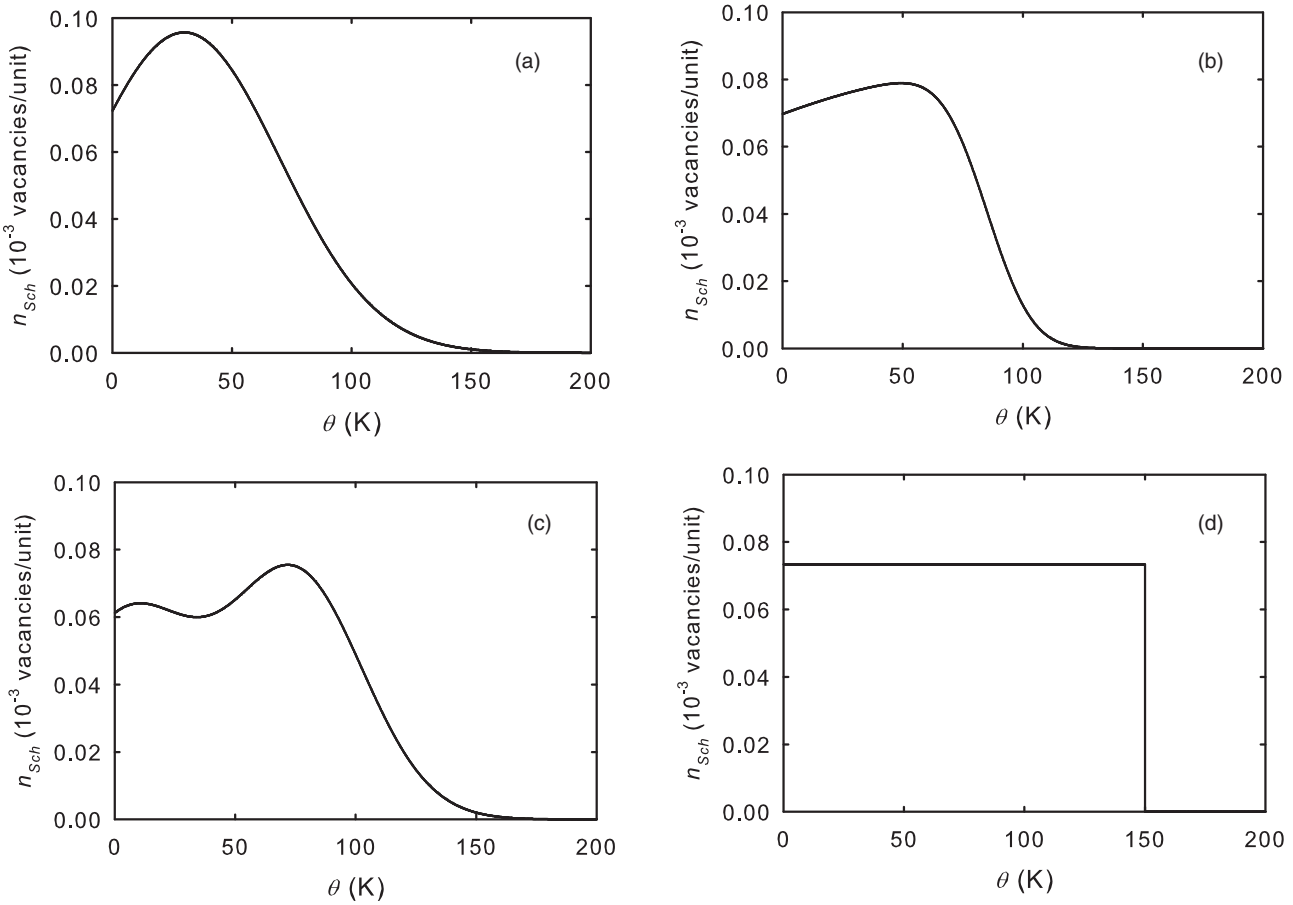

FIG. 2. Various possible distributions of energy gaps $n_{\mathrm{Sch}}(\theta)$ for the Schottky heat capacity arising from lattice vacancies. (a) Gaussian distribution. (b) Skewed Gaussian distribution. (c) Two Gaussian distributions summed. (d) Step distribution. See text for more details.

this distribution, n_{Sch} at $\theta = 30$ K corresponds to the average energy produced by vacancies that is more probable than the others perhaps due to the homogeneous nature inside the bulk of the material. The other energies arise because of the vacancies' proximity to grain boundaries, other vacancies, or the surface, which are generally less common than a homogeneous environment. This type of distribution might be suitable for large grain, crystalline materials.

A left-skewed Gaussian that has an average $\theta = 85$ K is shown in Fig. 2(b). The average here would again represent the vacancies in a homogeneous environment likely within the bulk of the material, but the skew would arise from a large concentration of vacancies near some similar inhomogeneous structure such as the surface. This distribution would likely apply to nanomaterials with a high surface-to-bulk ratio or materials with a high degree of disorder such as amorphous solids.

Figure 2(c) shows the sum of two Gaussian distributions that are centered at 5 and 75 K with standard deviations of 28 K. These Gaussians would be similar to the one discussed for Fig. 2(a), but here, we suppose the low-energy Gaussian arises from vacancies near or on the surface where there is less strain, and the high-energy Gaussian arises from the vacancies in the bulk of the material. This distribution may be more meaningful than the others because the center position, height, and width of each Gaussian can be varied as long as the sum has the same general shape. This allows for a different distribution for every sample that has a linear heat capacity and could therefore apply to any type of material.

A step distribution with a cutoff of $\theta = 150$ K (based on the experimental data outlined above) is shown in Fig. 2(d). This distribution is very similar to the constant value distribution used in Eq. (2) and assumes that the energies associated with the lattice vacancies are completely random and only exist below a particular energy, treating vacancies on the surface, in the bulk, and near defects or grain boundaries the same. The only variable factor in this distribution is the cutoff energy, which Anderson *et al.* [3] postulated to be related to the glass transition temperature on the order of 1000 K. Although this distribution simplifies calculations, it is unlikely that vacancies' energies will be completely random because bulk and surface energetics are so different [86], and a meaningful distribution must not ignore surface energies since many of the materials with linear terms are nanoparticles (see Table I).

B. Resultant heat capacity

When these distributions are used in Eq. (2), the resultant heat capacity as determined by numerical integration is approximately linear up to about 15 K and then gradually drops towards zero. Figure 3 shows the heat capacity curves (as C/T versus T in which a linear heat capacity will appear as a constant) that result from the distributions of Fig. 2. The Gaussian distribution yields a heat capacity that deviates

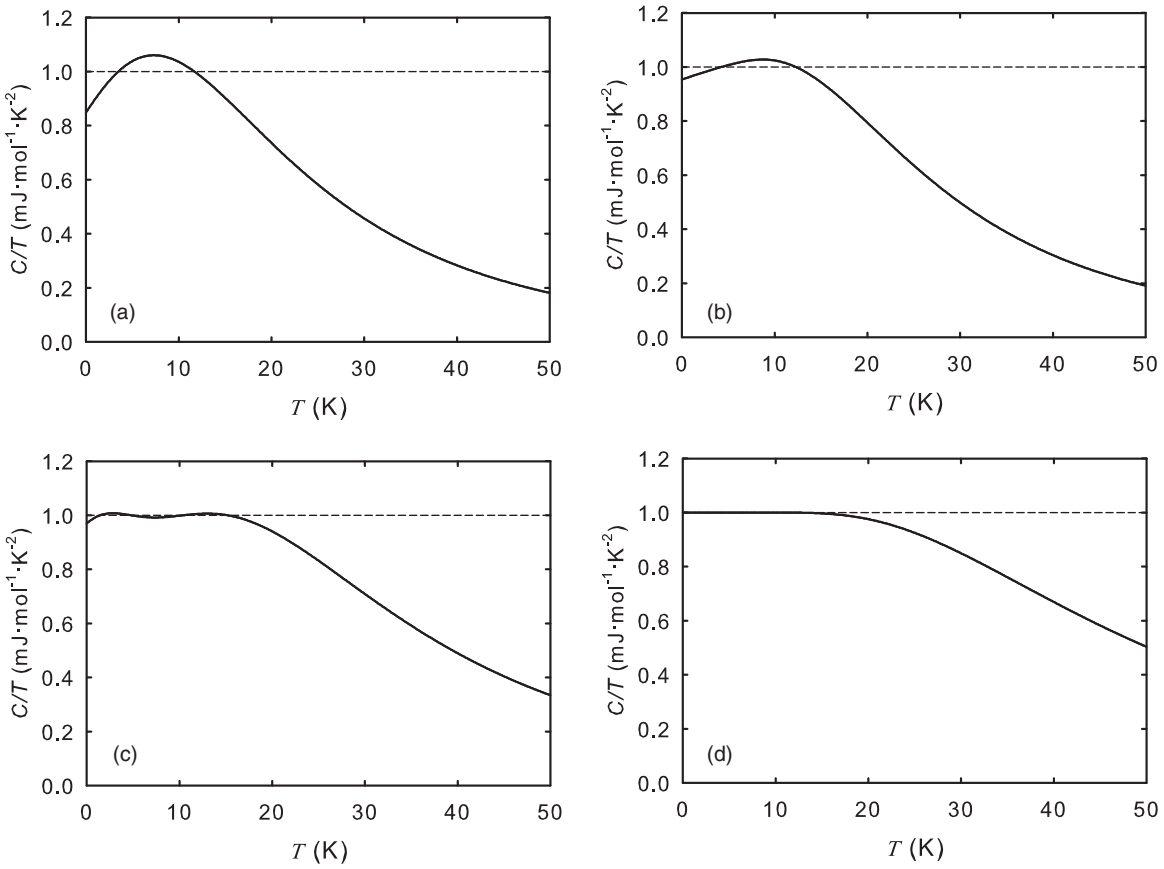

FIG. 3. Heat capacities generated by summing Schottky distributions that have n_{Sch} and θ values corresponding to the distributions: (a) Gaussian, (b) skewed Gaussian, (c) sum of two Gaussians, and (d) step (as seen in Fig. 2). Plots are of C/T; therefore, a linear heat capacity will be a constant in these plots.

the most from linearity (up to about 15%) as can be seen in Fig. 3(a). The heat capacity derived from the skewed Gaussian distribution, seen in Fig. 3(b), results in a heat capacity with less than a 5% deviation from linearity below 15 K. The distribution created by summing two Gaussian results in a heat capacity that deviates from linearity by less than 0.8% [see Fig. 3(c)], and the step distribution results in a heat capacity that deviates from linearity by about 0.05% below 10 K but increases to 0.3% by 15 K [see Fig. 3(d)]. For temperatures much less than the cutoff temperature, the step distribution produces the same linear heat capacity result of Eq. (2). All of these distributions resemble the energies typically produced from lattice vacancies and result in a heat capacity function that resembles what has been observed in many insulating materials, but the sum of two Gaussian distributions appears to be the most meaningful and has a high degree of linearity.

The distributions discussed above are just a few of the possible distributions that result in a linear heat capacity similar to what has been reported in the literature [3,23,34,44,51,52]. The actual distributions likely vary from the distributions presented here, but these distributions demonstrate the general shape that $n_{\mathrm{Sch}}(\theta)$ must have. Low-temperature heat capacity data can have an uncertainty of about 2%, and fits can have an uncertainty on the order of 1%; therefore, the nonlinearity of these derived heat capacities would likely be buried in the error of the data or fit. These results show that lattice vacancies do indeed produce a linear (or pseudolinear) contribution to the low-temperature heat capacity.

C. Quantification of vacancies from γ

Because each Schottky anomaly is a result of a lattice vacancy, the sum of all Schottky anomalies will give a measure of the total number of vacancies n_{vac} in a given sample. Finding n_{vac} is simply done by integrating the distribution $n_{\mathrm{Sch}}(\theta)$ over all θ. The height or normalization of the distribution will be manifest in the slope or linear term γ of the resultant heat capacity. We have calculated linear terms from typical vacancy concentrations of $n_{\mathrm{vac}} = 10^{-5}$ to 1 vacancies per formula unit (see Table II). Each distribution (see Fig. 2) was normalized to these values, and the linear term was determined by averaging the resultant heat capacity divided by temperature (C/T) from 0.5–15 K. These values were then used to determine constants of proportionality for each distribution by fitting to a line with zero intercept. The proportionalities are in the form $\gamma_{\mathrm{calc}} = c \times n_{\mathrm{vac}}$, and values of c were found to be 157, 151, 115, and 91 mJ mol^{-1} K^{-2} for the Gaussian, skewed Gaussian, two-Gaussian, and step distributions, respectively. These calculations have an estimated uncertainty of about 6% based on the heat capacity data, the fit, and the distribution's linearity, but with better data and fits, an uncertainty of about 2% would be reasonable.

D. Comparison to experimental data

To test the results of this model against actual data, we have measured the linear terms and vacancy concentrations of Co_3O_4, Co_3O_4 (n), CoO (n), Fe_3O_4 (n), CuO (n), and Al_2O_3 (n) which are part of separate, ongoing projects in our laboratory. The samples were found to have no chemical or phase impurities, and all characterization and thermodynamic data will be reported elsewhere.

The low-temperature heat capacities of Fe_3O_4 (n), CoO (n), and Al_2O_3 (n) and the experimental details have been published previously [19,20,41]. The other samples' heat capacities were measured on a Quantum Design Physical Properties Measurement System (PPMS) from 1.8–300 K following the method of Shi *et al.* [87]. Approximately 30 mg of each sample were mixed with copper strips (Alpha Aesar mass fraction purity 0.9995) to provide better thermal contact and put into copper cups that were pressed into pellets. Addenda measurements were performed that measured the heat capacity of the calorimeter and the grease used to attach the sample. After each addenda measurement, the sample was attached to the PPMS puck, and the heat capacity was measured. The system automatically corrects for the heat capacities of the calorimeter and grease, and the heat capacity of the copper was corrected for using data from Stevens and Boerio-Goates [88]. Data measured on the PPMS using this method have an estimated uncertainty of $\pm 0.02\, C_p^{\circ}$ for $2 < T/K < 10$ and $\pm 0.01\, C_p^{\circ}$ for $10 < T/K < 300$ [87]. The data below 10 K were fit to a theoretical function of the form

$$C(T) = \sum_{i=3,5,7} B_i T^i + \gamma T \,, \tag{4}$$

where the summation term represents the contribution from lattice vibrations, and the linear term is related to lattice vacancies. The fits having the same number of lattice terms but no linear contribution resulted in %RMS values of 7.16, 18.1, and 13.2 for Co_3O_4, Co_3O_4 (n), and CuO (n), respectively, whereas the fits including the linear term resulted in %RMS values of 0.82, 1.80, and 1.18. The values of γ obtained from the fits were 2.138, 14.111, and 0.489 mJ mol^{-1} K^{-2} for Co_3O_4, Co_3O_4 (n), and CuO (n), respectively (see Table I), and the approximated uncertainty in these values is 2.5% based on the heat capacity data and the fitting error.

The vacancy concentrations of Co_3O_4, Co_3O_4 (n), CoO (n), and Fe_3O_4 (n) were measured using a thermogravimetric reduction technique. Approximately 20 mg of each sample were placed in Pt crucibles which were inserted into a Mettler Toledo TGA/DSC 1 equipped with an automated GC 200 gas controller. To remove any surface-bound water, the samples were heated to 400 °C in He and cooled back to room temperature. The reduction gas was 10% H_2 in He with a flow rate of 100 mL min^{-1}, and the samples were heated at a rate of 3 °C min^{-1} to 900 °C. Reduction occurred abruptly at about 300 °C for the cobalt oxides and at about 400 for the iron oxide and resulted in mass losses of 26.531 0%, 25.972 6%, 18.50%, and 28.50% corresponding to stoichiometries of $Co_3O_{3.990\,5}$, $Co_3O_{3.877\,0}$ (n), $CoO_{0.836\,1}$ (n), and $Fe_{2.875\,0}O_4$ (n) respectively, yielding vacancy concentrations of $n_{\mathrm{vac}} = 0.009\,5, 0.123\,0, 0.163\,9$, and $0.125\,0$. The approximated uncertainty of these values is 15%.

The vacancy concentration of CuO (n) was determined by performing Rietveld refinement on powder x-ray diffraction (XRD) data collected at 100 K. CuO powder was packed into

a polyimide capillary with an inner diameter of 0.012 mm, and XRD data were collected in transmission mode using a MACH3 four-circle single-crystal diffractometer coupled to a Bruker Apex II CCD detector with a Bruker-Nonius FR591 rotating anode x-ray source producing Cu K_α radiation ($\lambda = 1.541\,8$ Å). Data were collected between 2–133° 2θ by performing a series of eight overlapping phi 360 scans. The Bruker XRD^2 program was used to merge the images and integrate the intensity of the diffraction rings. Rietveld refinement was performed using the PANalytical Highscore Plus software. The details of the analysis will be published elsewhere, but from the refinement, copper atoms were found to be slightly deficient yielding $Cu_{0.989\,1}O$ or $n_{vac} = 0.0109$, having an approximate uncertainty of 10%.

The vacancy concentration of Al_2O_3 (n) was determined using Eq. (3) and the value of E_v (0.18 eV) from Ref. [89]. Although the Al_2O_3 (n) samples used to determine γ were calcined at 973 K, we can assume that $T \approx 300$ K because the samples were cooled slowly to room temperature after calcination but were cooled quickly from room temperature to perform heat capacity measurements [41]. Using these values in Eq. (3) and accounting for the five atoms per formula unit gives an n_{vac} of 0.0047 moles of vacancies per mole of Al_2O_3 (n). The estimated uncertainty of n_{vac} determined using this method is 50%.

All these values of γ and n_{vac} are plotted in Fig. 4 along with the proportionalities derived herein. The plot shows how γ increases as n_{vac} increases. The error bars represent the uncertainties discussed above for each value of n_{vac}, and the uncertainty in γ of 2.5% is smaller than the size of the symbols. The deviations of the ratio of the actual values of γ and n_{vac} ($c = \gamma/n_{vac}$) from our calculations are 40% (using the Gaussian distribution) for Al_2O_3, 30% (using the Gaussian distribution) for Co_3O_4, 100% (using the step distribution) for CuO (n), 6.3% (using two-Gaussian distributions) for Co_3O_4 (n), 230% (using the step distribution) for Fe_3O_4 (n), 150% (using the step distribution) for CoO (n).

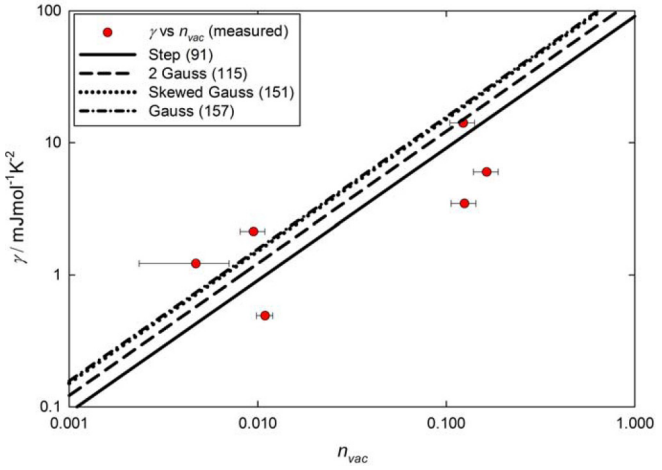

FIG. 4. (Color online) γ versus n_{vac} of several samples. From left to right: Al_2O_3 (n), Co_3O_4, CuO (n), Co_3O_4 (n), Fe_3O_4 (n), and CoO (n). Also shown are the lines derived from the four distributions of Schottky anomalies with the slopes (units of millijoules per mole per Kelvin) shown in parentheses in the legend.

The experimental values of γ and n_{vac} differ from our theoretical values by at most a factor of two or three and as little as a few percent. When all the uncertainties are taken into account, these calculations show qualitative agreement as well as quantitative agreement, providing further evidence that the linear term of insulating materials does indeed stem from lattice vacancies. As further evidence supporting our claims, we note that the differences between the measured and calculated values of γ from n_{vac} are similar despite the method used to determine n_{vac}.

E. Trends in γ and n_{vac}

As a final note, we recognize several trends emphasizing our conclusions. All values of γ found in Table I lie between 0.01 and 100 mJ mol^{-1} K^{-2}, and values of n_{vac} in Table II lie between 10^{-5} and 1, which is the same range of values we would expect when applying our calculations to γ. Values of γ for nanophase TiO_2, CoO, Co_3O_4, α-Fe_2O_3, CuO, SnO_2, and ZnO are all larger than the bulk phase values of γ. Values of n_{vac} from Table II also increase as particle size decreases for CeO_2 and Fe_3O_4. The Co-doped ZnO and Al-doped TiO_2 systems have γ much greater than what would be expected for a simple CoO/ZnO or Al_2O_3/TiO_2 mixture, and values of n_{vac} for TiO_2 are also larger when dopants are present. Mitchell [72] has also shown that the concentration of defects increases with increasing dopant concentrations.

III. CONCLUSION

We have shown that the linear term, which is often necessary to fit the low-temperature heat capacity data for nonmetallic materials, is related to the number of lattice vacancies. We have created several distributions of $n_{Sch}(\theta)$ that have similar energy cutoffs to experimental data from the literature and are physically meaningful. The vacancy energies associated with these distributions are assumed to result in small Schottky anomalies due to a puckering of the lattice. These distributions have been shown to produce a linear heat capacity similar to what has been observed for these kinds of materials. We have measured values of γ and n_{vac} of several samples and compared those to our theoretical values. These values show qualitative and quantitative agreement with our model, and linear terms and lattice vacancy concentrations have been shown to have many similar trends, providing further evidence for our arguments. This paper provides meaningful evidence supporting the claim that the linear term in insulating materials results from lattice vacancies.

ACKNOWLEDGMENTS

We would like to thank Kamyar Keyvanloo and McCallin Fisher for help with the TGA experiments and Dr. Stacey Smith for help with the XRD experiment. This paper was financially supported by a grant from the US Department of Energy under Grant No. DE-FG02-05ER15666.

[1] E. S. R. Gopal, *Specific Heats at Low Temperatures* (Plenum Press, New York, 1966), Vol. 227.

[2] C. Kittel and P. McEuen, *Introduction to Solid State Physics* (Wiley, New York, 1996), Vol. 7.

[3] P. W. Anderson, B. Halperin, and C. M. Varma, Anomalous low-temperature thermal properties of glasses and spin glasses, Philos. Mag. **25**, 1 (1972).

[4] N. E. Phillips, J. P. Emerson, R. A. Fisher, J. E. Gordon, B. F. Woodfield, and D. A. Wright, Is there an intrinsic linear term in the specific heat of $YBa_2Cu_3O_7$?, Physica C **235–240**, Part 3, 1737 (1994).

[5] J. M. D. Coey, S. Von Molnar, and A. Torressen, Low-temperature specific heat of $Bi_2Sr_2CaCu_2O_8$: Comparison with some other layered oxides, J. Less-Common Met. **151**, 191 (1989).

[6] J. Bardeen, L. N. Cooper, and J. R. Schrieffer, Theory of superconductivity, Phys. Rev. **108**, 1175 (1957).

[7] R. Fisher, J. Gordon, and N. Phillips, Specific heat of the high-T_c oxide superconductors, J. Supercond. **1**, 231 (1988).

[8] N. E. Phillips, R. A. Fisher, J. E. Gordon, S. Kim, A. M. Stacy, M. K. Crawford, and E. M. McCarron III, Specific heat of $YBa_2Cu_3O_7$: Origin of the "linear" term and volume fraction of superconductivity, Phys. Rev. Lett. **65**, 357 (1990).

[9] D. A. Wright, J. P. Emerson, B. F. Woodfield, J. E. Gordon, R. A. Fisher, and N. E. Phillips, Low-temperature specific heat of $YBa_2Cu_3O_{7-\delta}$, $0 \leqslant \delta \leqslant 0.2$: Evidence for d-wave pairing, Phys. Rev. Lett. **82**, 1550 (1999).

[10] N. E. Phillips, J. P. Emerson, R. A. Fisher, J. E. Gordon, B. F. Woodfield, and D. A. Wright, Specific heat of $YBa_2Cu_3O_7$, J. Supercond. **7**, 251 (1994).

[11] B. Golding, N. O. Birge, W. H. Haemmerle, R. J. Cava, and E. Rietman, Tunneling systems in superconducting $YBa_2Cu_3O_7$, Phys. Rev. B **36**, 5606 (1987).

[12] D. Eckert, A. Junod, A. Bezinge, T. Graf, and J. Muller, Low-temperature specific heat of $YBa_2Cu_3O_7$, $YBa_2Cu_3O_6$, Y_2BaCuO_5, $YBa_3Cu_2O_7$, $BaCuO_2$, and CuO, J. Low Temp. Phys. **73**, 241 (1988).

[13] K. A. Moler, D. L. Sisson, J. S. Urbach, M. R. Beasley, A. Kapitulnik, D. J. Baar, R. Liang, and W. N. Hardy, Specific heat of $YBa_2Cu_3O_{7-\delta}$, Phys. Rev. B **55**, 3954 (1997).

[14] D. A. Wright, J. P. Emerson, B. F. Woodfield, S. F. Reklis, J. E. Gordon, R. A. Fisher, and N. E. Phillips, Dependence of the low-temperature specific heat of $YBa_2Cu_3O_{7-\delta}$ on δ and magnetic field: The $H^{1/2}T$ term for $H \neq 0$; absence of evidence for a T^2 term for $H = 0$, J. Low Temp. Phys. **105**, 897 (1996).

[15] J. P. Emerson, D. A. Wright, B. F. Woodfield, J. E. Gordon, R. A. Fisher, and N. E. Phillips, Specific heat of $YBa_2Cu_3O_{7-\delta}$, $0 \leqslant \delta \leqslant 0.2$: Concentrations of paramagnetic centers and values of other parameters as functions of δ, Phys. Rev. Lett. **82**, 1546 (1999).

[16] R. McCallum, D. Johnston, C. Luengo, and M. Maple, Superconducting and normal state properties of $Li_{1+x}Ti_{2-x}O_4$ spinel compounds. II. Low-temperature heat capacity, J. Low Temp. Phys. **25**, 177 (1976).

[17] K. Kumagai, Y. Nakamichi, I. Watanabe, Y. Nakamura, H. Nakajima, N. Wada, and P. Lederer, Linear temperature term of heat capacity in insulating and superconducting La-Ba-Cu-O systems, Phys. Rev. Lett. **60**, 724 (1988).

[18] A. Junod, D. Eckert, G. Triscone, J. Müller, and W. Reichardt, A study of the magnetic transitions in CuO: Specific heat (1-330 K), magnetic susceptibility and phonon density of states, J. Phys.: Condens. Matter **1**, 8021 (1989).

[19] C. L. Snow, Q. Shi, J. Boerio-Goates, and B. F. Woodfield, Heat capacity studies of nanocrystalline magnetite (Fe_3O_4), J. Phys. Chem. C **114**, 21100 (2010).

[20] L. Wang, K. Vu, A. Navrotsky, R. Stevens, B. F. Woodfield, and J. Boerio-Goates, Calorimetric study: Surface energetics and the magnetic transition in nanocrystalline CoO, Chem. Mater. **16**, 5394 (2004).

[21] J. C. Lashley, R. Stevens, M. K. Crawford, J. Boerio-Goates, B. F. Woodfield, Y. Qiu, J. W. Lynn, P. A. Goddard, and R. A. Fisher, Specific heat and magnetic susceptibility of the spinels $GeNi_2O_4$ and $GeCo_2O_4$, Phys. Rev. B **78**, 104406 (2008).

[22] S. J. Smith, R. Stevens, S. Liu, G. Li, A. Navrotsky, J. Boerio-Goates, and B. F. Woodfield, Heat capacities and thermodynamic functions of TiO_2 anatase and rutile: Analysis of phase stability, Am. Mineral. **94**, 236 (2009).

[23] R. A. Fisher, D. A. Wright, J. P. Emerson, B. F. Woodfield, N. E. Phillips, Z. R. Wang, and D. C. Johnston, Low-temperature specific heat of $BaCuO_2$ and $BaCuO_{2.14}$ in magnetic fields to 7 T, Phys. Rev. B **61**, 538 (2000).

[24] B. K. Chakraverty, M. J. Sienko, and J. Bonnerot, Low-temperature specific heat and magnetic susceptibility of nonmetallic vanadium bronzes, Phys. Rev. B **17**, 3781 (1978).

[25] J. M. D. Coey, M. Viret, L. Ranno, and K. Ounadjela, Electron localization in mixed-valence manganites, Phys. Rev. Lett. **75**, 3910 (1995).

[26] J. Majzlan, A. Navrotsky, B. F. Woodfield, B. E. Lang, J. Boerio-Goates, and R. A. Fisher, Phonon, spin-wave, and defect contributions to the low-temperature specific heat of α-FeOOH, J. Low Temp. Phys. **130**, 69 (2003).

[27] C. L. Snow, S. J. Smith, B. E. Lang, Q. Shi, J. Boerio-Goates, B. F. Woodfield, and A. Navrotsky, Heat capacity studies of the iron oxyhydroxides akaganéite (β-FeOOH) and lepidocrocite (γ-FeOOH), J. Chem. Thermodyn. **43**, 190 (2011).

[28] R. Stephens, Low-temperature specific heat and thermal conductivity of noncrystalline dielectric solids, Phys. Rev. B **8**, 2896 (1973).

[29] J. M. Schliesser, S. J. Smith, G. Li, L. Li, T. F. Walker, T. Parry, J. Boerio-Goates, and B. F. Woodfield, Heat capacity and thermodynamic functions of nano-TiO_2 anatase in relation to bulk-TiO_2 anatase, J. Chem. Thermodyn. **81**, 298 (2015).

[30] J. M. Schliesser, S. J. Smith, G. Li, L. Li, T. F. Walker, T. Parry, J. Boerio-Goates, and B. F. Woodfield, Heat capacity and thermodynamic functions of nano-TiO_2 rutile in relation to bulk-TiO_2 rutile, J. Chem. Thermodyn. **81**, 311 (2015).

[31] C. L. Snow, C. R. Lee, Q. Shi, J. Boerio-Goates, and B. F. Woodfield, Size-dependence of the heat capacity and thermodynamic properties of hematite (α-Fe_2O_3), J. Chem. Thermodyn. **42**, 1142 (2010).

[32] C. Snow, K. Lilova, A. Radha, Q. Shi, S. Smith, A. Navrotsky, J. Boerio-Goates, and B. Woodfield, Heat capacity and thermodynamics of a synthetic two-line ferrihydrite, FeOOH·0.027 H_2O, J. Chem. Thermodyn. **58**, 307 (2013).

[33] C. L. Snow, Q. Shi, J. Boerio-Goates, and B. F. Woodfield, Heat capacity, third-law entropy, and low-temperature physical behavior of bulk hematite (α-Fe_2O_3), J. Chem. Thermodyn. **42**, 1136 (2010).

[34] Q. Shi, L. Zhang, M. E. Schlesinger, J. Boerio-Goates, and B. F. Woodfield, Low temperature heat capacity study of $Fe(PO_3)_3$ and $Fe_2P_2O_7$, J. Chem. Thermodyn. **61**, 51 (2013).

[35] Q. Shi, L. Zhang, M. E. Schlesinger, J. Boerio-Goates, and B. F. Woodfield, Low temperature heat capacity study of Fe_3PO_7 and $Fe_4(P_2O_7)_3$, J. Chem. Thermodyn. **62**, 86 (2013).

[36] Q. Shi, L. Zhang, M. E. Schlesinger, J. Boerio-Goates, and B. F. Woodfield, Low temperature heat capacity study of $FePO_4$ and $Fe_3(P_2O_7)_2$, J. Chem. Thermodyn. **62**, 35 (2013).

[37] Q. Shi, J. Boerio-Goates, K. Woodfield, M. Rytting, K. Pulsipher, E. C. Spencer, N. L. Ross, A. Navrotsky, and B. F. Woodfield, Heat capacity studies of surface water confined on cassiterite (SnO_2) nanoparticles, J. Phys. Chem. C **116**, 3910 (2012).

[38] C. Ma, Q. Shi, B. F. Woodfield, and A. Navrotsky, Low temperature heat capacity of bulk and nanophase ZnO and $Zn_{1-x}Co_xO$ wurtzite phases, J. Chem. Thermodyn. **60**, 191 (2013).

[39] W. Zhou, Q. Shi, B. F. Woodfield, and A. Navrotsky, Heat capacity of hafnia at low temperature, J. Chem. Thermodyn. **43**, 970 (2011).

[40] Q. Shi, T.-J. Park, J. Schliesser, A. Navrotsky, and B. F. Woodfield, Low temperature heat capacity study of $Ba_2TiSi_2O_8$ and $Sr_2TiSi_2O_8$, J. Chem. Thermodyn. **72**, 77 (2014).

[41] E. C. Spencer, B. Huang, S. F. Parker, A. I. Kolesnikov, N. L. Ross, and B. F. Woodfield, The thermodynamic properties of hydrated γ-Al_2O_3 nanoparticles, J. Chem. Phys. **139**, 244705 (2013).

[42] R. E. Olsen, T. M. Alam, C. H. Bartholomew, D. B. Enfield, J. Schliesser, and B. F. Woodfield, Structure analysis of Al-modified TiO_2 nanocatalyst supports, J. Phys. Chem. C **118**, 9176 (2014).

[43] M. A. Ribeiro da Silva, M. D. Ribeiro da Silva, A. I. Lobo Ferreira, Q. Shi, B. F. Woodfield, and R. N. Goldberg, Thermochemistry of α-D-xylose(cr), J. Chem. Thermodyn. **58**, 20 (2013).

[44] J.-Y. Genoud, A. Mirmelstein, G. Triscone, A. Junod, and J. Muller, Phase stability and low-temperature specific heat up to 14 T of $BaCuO_x$ as a function of oxygen stoichiometry, Phys. Rev. B **52**, 12833 (1995).

[45] A. Andreev and I. Lifshits, Quantum theory of defects in crystals, Sov. Phys. JETP **29**, 1107 (1969).

[46] H. B. Rosenstock, Anomalous specific heat of glasses: Its temperature dependence, J. Non-Cryst. Solids **7**, 123 (1972).

[47] R. A. Fisher, Anomalous heat capacity of vitreous silica: Effect of interstitial ^{4}He, J. Non-Cryst. Solids **41**, 251 (1980).

[48] W. Phillips, Tunneling states in amorphous solids, J. Low Temp. Phys. **7**, 351 (1972).

[49] W. Phillips, Two-level states in glasses, Rep. Prog. Phys. **50**, 1657 (1987).

[50] J. Xu, J. Tang, K. Sato, Y. Tanabe, H. Miyasaka, M. Yamashita, S. Heguri, and K. Tanigaki, Low-temperature heat capacity of $Sr_8Ga_{16}Ge_{30}$ and $Ba_8Ga_{16}Ge_{30}$: Tunneling states and electron-phonon interaction in clathrates, Phys. Rev. B **82**, 085206 (2010).

[51] D. McWhan, C. Varma, F. Hsu, and J. Remeika, Low-temperature heat capacity of alkali-metal and silver β-aluminas, Phys. Rev. B **15**, 553 (1977).

[52] T. Sandin and P. Keesom, Specific heat and paramagnetic susceptibility of stoichiometric and reduced rutile (TiO_2) from 0.3 to 20 K, Phys. Rev. **177**, 1370 (1969).

[53] Z. L. Wang, J. S. Yin, and Y. D. Jiang, EELS analysis of cation valence states and oxygen vacancies in magnetic oxides, Micron **31**, 571 (2000).

[54] L. Liu, T. Lee, L. Qiu, Y. Yang, and A. Jacobson, A thermogravimetric study of the phase diagram of strontium cobalt iron oxide, $SrCo_{0.8}Fe_{0.2}O_{3-\delta}$, Mater. Res. Bull. **31**, 29 (1996).

[55] J. Mizusaki, Y. Mima, S. Yamauchi, K. Fueki, and H. Tagawa, Nonstoichiometry of the perovskite-type oxides $La_{1-x}Sr_xCoO_{3-\delta}$, J. Solid State Chem. **80**, 102 (1989).

[56] M. H. Lankhorst, H. Bouwmeester, and H. Verweij, High-temperature coulometric titration of $La_{1-x}Sr_xCoO_{3-\delta}$: Evidence for the effect of electronic band structure on non-stoichiometry behavior, J. Solid State Chem. **133**, 555 (1997).

[57] Y. D. Tretyakov, V. Komarov, N. Prosvirnina, and I. Kutsenok, Nonstoichiometry and defect structures in copper oxides and ferrites, J. Solid State Chem. **5**, 157 (1972).

[58] Y. Matsuda, M. Karppinen, Y. Yamazaki, and H. Yamauchi, Oxygen-vacancy concentration in $A_2MgMoO_{6-\delta}$ double-perovskite oxides, J. Solid State Chem. **182**, 1713 (2009).

[59] S. McIntosh, J. F. Vente, W. G. Haije, D. H. A. Blank, and H. J. M. Bouwmeester, Oxygen stoichiometry and chemical expansion of $Ba_{0.5}Sr_{0.5}Co_{0.8}Fe_{0.2}O_{3-\delta}$ measured by in situ neutron diffraction, Chem. Mater. **18**, 2187 (2006).

[60] I. Kosacki, T. Suzuki, H. U. Anderson, and P. Colomban, Raman scattering and lattice defects in nanocrystalline CeO_2 thin films, Solid State Ionics **149**, 99 (2002).

[61] Q. Wu, Q. Zheng, and R. van de Krol, Creating oxygen vacancies as a novel strategy to form tetrahedrally coordinated Ti^{4+} in Fe/TiO_2 Nanoparticles, J. Phys. Chem. C **116**, 7219 (2012).

[62] Z. L. Wang, J. Yin, Y. Jiang, and J. Zhang, Studies of Mn valence conversion and oxygen vacancies in LaCaMnO using electron energy-loss spectroscopy, Appl. Phys. Lett. **70**, 3362 (1997).

[63] T. Mayer, J. Elam, S. George, P. Kotula, and R. Goeke, Atomic-layer deposition of wear-resistant coatings for microelectromechanical devices, Appl. Phys. Lett. **82**, 2883 (2003).

[64] Y.-M. Kim, J. He, M. D. Biegalski, H. Ambaye, V. Lauter, H. M. Christen, S. T. Pantelides, S. J. Pennycook, S. V. Kalinin, and A. Y. Borisevich, Probing oxygen vacancy concentration and homogeneity in solid-oxide fuel-cell cathode materials on the subunit-cell level, Nat. Mater. **11**, 888 (2012).

[65] C. S. Enache, J. Schoonman, and R. Van Krol, The photoresponse of iron- and carbon-doped TiO_2 (anatase) photoelectrodes, J. Electroceram. **13**, 177 (2004).

[66] Y. Chiang, E. Lavik, I. Kosacki, H. Tuller, and J. Ying, Nonstoichiometry and electrical conductivity of nanocrystalline CeO_{2-x}, J. Electroceram. **1**, 7 (1997).

[67] M. Janousch, G. I. Meijer, U. Staub, B. Delley, S. F. Karg, and B. P. Andreasson, Role of oxygen vacancies in Cr-doped $SrTiO_3$ for resistance-change memory, Adv. Mater. **19**, 2232 (2007).

[68] J.-H. Hwang and T. O. Mason, Defect chemistry and transport properties of nanocrystalline cerium oxide, Z. Phys. Chem. **207**, 21 (1998).

[69] K. L. Duncan, Y. Wang, S. R. Bishop, F. Ebrahimi, and E. D. Wachsman, Role of point defects in the physical properties of fluorite oxides, J. Am. Ceram. Soc. **89**, 3162 (2006).

[70] F. Schedin, E. Hill, G. Van der Laan, and G. Thornton, Magnetic properties of stoichiometric and nonstoichiometric ultrathin Fe_3O_4(111) films on Al_2O_3(0001), J. Appl. Phys. **96**, 1165 (2004).

[71] M. O'Keeffe and W. J. Moore, Thermodynamics of the formation and migration of defects in cuprous oxide, J. Chem. Phys. **36**, 3009 (1962).

[72] T. E. Mitchell, Dislocations and mechanical properties of MgO-Al_2O_3 spinel single crystals, J. Am. Ceram. Soc. **82**, 3305 (1999).

[73] J. W. Koenitzer, P. H. Keesom, and J. M. Honig, Heat capacity of magnetite in the range 0.3 to 10 K, Phys. Rev. B **39**, 6231 (1989).

[74] A. S. Mysovsky, P. V. Sushko, S. Mukhopadhyay, A. H. Edwards, and A. L. Shluger, Calibration of embedded-cluster method for defect studies in amorphous silica, Phys. Rev. B **69**, 085202 (2004).

[75] M. Boero, A. Pasquarello, J. Sarnthein, and R. Car, Structure and hyperfine parameters of E_1' centers in α-quartz and in vitreous SiO_2, Phys. Rev. Lett. **78**, 887 (1997).

[76] C. G. Van de Walle and P. E. Blöchl, First-principles calculations of hyperfine parameters, Phys. Rev. B **47**, 4244 (1993).

[77] P. E. Blöchl, First-principles calculations of defects in oxygen-deficient silica exposed to hydrogen, Phys. Rev. B **62**, 6158 (2000).

[78] J. Boerio-Goates, S. J. Smith, S. Liu, B. E. Lang, G. Li, B. F. Woodfield, and A. Navrotsky, Characterization of surface defect sites on bulk and nanophase anatase and rutile TiO_2 by low-temperature specific heat, J. Phys. Chem. C **117**, 4544 (2013).

[79] C. Di Valentin, A. Tilocca, A. Selloni, T. Beck, A. Klust, M. Batzill, Y. Losovyj, and U. Diebold, Adsorption of water on reconstructed rutile TiO_2(011)-(2×1): Ti=O double bonds and surface reactivity, J. Am. Chem. Soc. **127**, 9895 (2005).

[80] D. Smith, Hindered rotation of the ammonium ion in the solid state, Chem. Rev. **94**, 1567 (1994).

[81] J. C. M. Li and K. S. Pitzer, Energy levels and thermodynamic functions for molecules with internal rotation. IV. Extended tables for molecules with small moments of inertia, J. Phys. Chem. **60**, 466 (1956).

[82] L. Skuja, Optically active oxygen-deficiency-related centers in amorphous silicon dioxide, J. Non-Cryst. Solids **239**, 16 (1998).

[83] U. Buchenau, N. Nücker, and A. J. Dianoux, Neutron scattering study of the low-frequency vibrations in vitreous silica, Phys. Rev. Lett. **53**, 2316 (1984).

[84] D. Gryaznov, E. Blokhin, A. Sorokine, E. A. Kotomin, R. A. Evarestov, A. Bussmann-Holder, and J. Maier, A comparative *ab initio* thermodynamic study of oxygen vacancies in ZnO and $SrTiO_3$: Emphasis on phonon contribution, J. Phys. Chem. C **117**, 13776 (2013).

[85] P. Colomban, F. Romain, A. Neiman, and I. Animitsa, Double perovskites with oxygen structural vacancies: Raman spectra, conductivity and water uptake, Solid State Ionics **145**, 339 (2001).

[86] B. Huang, J. Schliesser, R. E. Olsen, S. J Smith, and B. F Woodfield, Synthesis and thermodynamics of porous metal oxide nanomaterials, Curr. Inorg. Chem. **4**, 40 (2014).

[87] Q. Shi, J. Boerio-Goates, and B. F. Woodfield, An improved technique for accurate heat capacity measurements on powdered samples using a commercial relaxation calorimeter, J. Chem. Thermodyn. **43**, 1263 (2011).

[88] R. Stevens and J. Boerio-Goates, Heat capacity of copper on the ITS-90 temperature scale using adiabatic calorimetry, J. Chem. Thermodyn. **36**, 857 (2004).

[89] I. Tanaka, F. Oba, K. Tatsumi, M. Kunisu, M. Nakano, and H. Adachi, Theoretical formation energy of oxygen-vacancies in oxides, Mater. Trans. **43**, 1426 (2002).